Noname manuscript No.
(will be inserted by the editor)

Non-stationary structure-preserving preconditioning for image restoration

Pietro Dell'Acqua · Marco Donatelli · Lothar Reichel

Received: date / Accepted: date

Abstract Non-stationary regularizing preconditioners have recently been proposed for the acceleration of classical iterative methods for the solution of linear discrete ill-posed problems. This paper explores how these preconditioners can be combined with the flexible GMRES iterative method. A new structure-respecting strategy to construct a sequence of regularizing preconditioners is proposed. We show that flexible GMRES applied with these preconditioners is able to restore images that have been contaminated by strongly non-symmetric blur, while several other iterative methods fail to do this.

Keywords image deblurring · non-stationary preconditioning · flexible GMRES

1 Introduction

We are concerned with the restoration of blurred and noise-corrupted images in two space-dimensions. The blurring is modeled by a convolution and the image degradation model is of the form

$$g(\boldsymbol{x}) = [Kf](\boldsymbol{x}) + \nu(\boldsymbol{x}) = \int_{\mathbb{R}^2} h(\boldsymbol{x}-\boldsymbol{y}) f(\boldsymbol{y}) \mathrm{d}\boldsymbol{y} + \nu(\boldsymbol{x}), \qquad \boldsymbol{x} \in \Omega \subset \mathbb{R}^2, \quad (1)$$

where f represents the (desired but unavailable) exact image, h the space invariant point-spread function (PSF) with compact support, ν random noise, and g the

Pietro Dell'Acqua
Facoltà di Scienze e Tecnologie Informatiche
Libera Università di Bolzano, Bolzano (Italy)
E-mail: pietro.dellacqua@gmail.com

Marco Donatelli
Dipartimento di Scienza e Alta Tecnologia,
Università degli Studi dell'Insubria, Como (Italy)
E-mail: marco.donatelli@uninsubria.it

Lothar Reichel
Department of Mathematical Sciences
Kent State University, Kent, OH (USA)
E-mail: reichel@math.kent.edu

(available) blurred and noise-corrupted image. Hence, f and g are real-valued non-negative functions that determine the light intensity of the desired and available images, respectively.

Discretization of the integral equation (1) at equidistant nodes gives the linear system of algebraic equations

$$g_i = \sum_{j \in \mathbb{Z}^2} h_{i-j} f_j + \nu_i, \qquad i \in \mathbb{Z}^2. \tag{2}$$

The entries of the discrete images $\boldsymbol{g} = [g_i]$ and $\boldsymbol{f} = [f_j]$ represent the light intensity at each picture element (pixel) and $\boldsymbol{\nu} = [\nu_i]$ models the noise-contamination at these pixels. The pixels with index $i \in [1, n]^2$ make up the finite field of view (FOV), which for notational simplicity is assumed to be square. We would like to determine an accurate approximation of the exact image $\boldsymbol{f}$ in the FOV given $\boldsymbol{h} = [h_i]$, distributional information about $\boldsymbol{\nu}$, and the blurred image $\boldsymbol{g}$ in the FOV.

The linear system of algebraic equations defined by (2) with i restricted to $[1, n]^2$ is underdetermined when there are non-vanishing coefficients h_i with $i \neq 0$, because then there are n^2 equations, while the number of unknowns is larger. A common approach to determine a meaningful solution of this kind of underdetermined system is to impose boundary conditions on the image to obtain a linear system of algebraic equations with a square matrix,

$$A\boldsymbol{f} = \boldsymbol{g}, \qquad A \in \mathbb{R}^{n^2 \times n^2}, \qquad \boldsymbol{f}, \boldsymbol{g} \in \mathbb{R}^{n^2}. \tag{3}$$

The boundary conditions specify that the f_j-values in (2) at pixels outside the FOV are linear combinations of f_j-values at certain pixels inside the FOV. Popular boundary conditions include zero Dirichlet boundary conditions (ZDBCs), periodic boundary conditions (PBCs), reflective boundary conditions (RBCs) discussed in [28], and anti-reflective boundary conditions (ARBCs) proposed in [33]. Detailed descriptions and analyses of these boundary conditions can be found in [15, 24, 25]. This paper focuses on ARBCs, which yield an accurate model and often allow simple implementation. We restrict our attention to ARBCs only for the sake of simplicity, but we remark that more accurate boundary conditions and other strategies for dealing with boundary artifacts recently have been proposed in the literature, see [6, 10, 18, 29], and can be applied to construct preconditioners as well. Theoretical results on optimal preconditioning for ARBCs are discussed in [9].

Due to the space-invariance of the PSF, the matrix A has a block Toeplitz-type structure. The detailed structure depends on the boundary conditions. For instance, ZDBCs give a block-Toeplitz-Toeplitz-block (BTTB) structure, while PBCs make A a block-circulant-circulant-block (BCCB) matrix. This is discussed in more detail below.

Quadrantally symmetric PSFs, i.e., PSFs that are symmetric with respect to both the horizontal and vertical axes, arise, e.g., when modeling symmetric Gaussian blur. The associated matrix A in (3) allows diagonalization by a fast transform when RBCs or ARBCs are imposed. These transforms can be applied to develop fast methods for the approximate solution of (3); see [1, 5, 28].

For symmetric PSFs, the matrix A is symmetric and many iterative regularization methods can be applied to the approximate solution of (3), such as non-stationary iterative methods and variants of the minimal residual method; see

[12,16]. On the other hand, for strongly non-symmetric PSFs specially designed iterative regularization methods have to be applied; see [14,20] for illustrations.

The matrix A in (3) generally is severely ill-conditioned and may be numerically rank-deficient. We refer to linear system of equations (3) with such a matrix as linear discrete ill-posed problems. Due to the error in the right-hand side vector $\boldsymbol{g}$ in (3), which is caused by the noise $\boldsymbol{\nu}$ in (2), and because of the ill-conditioning of the matrix, one generally is not interested in the exact solution of (3) (if it exists). Instead one typically would like to compute a suitable approximate solution that furnishes an accurate approximation of the desired image $\boldsymbol{f}$. Such an approximate solution can be computed by regularizing the system of equations (3), e.g., by replacing this system by a nearby one, whose solution is less sensitive to the error in $\boldsymbol{g}$. Regularization methods require the choice of a regularization parameter that determines the amount of regularization.

The present paper is concerned with the development of fast and stable iterative regularization methods for the approximate solution of (3) when the matrix A is defined by a non-symmetric PSF h with ARBCs. In particular, we focus on GMRES-type iterative methods. The (standard) GMRES method is commonly used for the iterative solution of large linear systems of equations with a square non-symmetric matrix that is obtained by the discretization of a well-conditioned problem, such as an elliptic partial differential equation with Dirichlet boundary conditions. In this context, preconditioners are employed to accelerate the convergence of the iterative method. An advantage of GMRES, when compared to other iterative methods such as CGLS, is that GMRES does not require the evaluation of matrix-vector products with A^T, the transpose of A. This is commented on further in Section 3.

Preconditioners applied to the iterative solution of linear discrete ill-posed problems (3) should avoid propagating the error $\boldsymbol{\nu}$ in $\boldsymbol{g}$ into the the computed approximate solution. We will show that such preconditioners can be determined by incorporating a threshold parameter in their definition. Note that the preconditioning strategy for GMRES proposed in [14] can determine accurate restorations, but may require many iterations when the noise level is low. In fact, typically linear discrete ill-posed problems of the form (3) are more difficult to solve when the noise level is low than when it is high, because the restoration of the former kind of images generally requires more iterations.

We would like to investigate the use of non-stationary preconditioning with GMRES-type methods with the aim to obtain accurate restorations within only a few iterations also when the noise level is low and the PSF is strongly non-symmetric. Instead of solving right-preconditioned systems of the form

$$AP\boldsymbol{z} = \boldsymbol{g}, \qquad \boldsymbol{z} = P^{-1}\boldsymbol{f} \tag{4}$$

by GMRES, we propose to use the flexible GMRES (F-GMRES) method first described by Saad [30] to solve, at step k,

$$AP_k\boldsymbol{z} = \boldsymbol{g}, \qquad \boldsymbol{z} = P_k^{-1}\boldsymbol{f}, \tag{5}$$

where the preconditioner P_k is modified in each iteration. The application of F-GMRES to the solution of linear discrete ill-posed problems has previously been discussed by Gazzola and Nagy [19] and Morikuni et al. [27]. The preconditioners developed in the present paper are new. Exploiting the tools developed within

the framework of preconditioned Landweber iterative methods [7,8], we define preconditioners for F-GMRES. By using a suitable sequence of preconditioners P_k in (5), we obtain a preconditioned F-GMRES method that is well suited for image restoration. The preconditioner P_k depends on a thresholding parameter α_k, whose choice will be discussed in Section 3.

Several other preconditioning techniques for linear systems of algebraic equations that arise in image restoration and have a square BTTB-type matrix have been described in the literature; see, e.g., [7,14,17,20,22,23] and references therein. In all available preconditioning techniques, the preconditioner P is chosen before the iterations are begun and kept fixed during the computations. This corresponds to applying an iterative method to the preconditioned system (4). A nice recent survey is presented by Gazzola et al. [21]. However, it may be difficult to choose a suitable preconditioner before the start of the iterations. Our approach circumvents this complication by allowing the preconditioner to be updated during the solution process.

This paper is organized as follows. Section 2 contains a brief overview of anti-reflective boundary conditions. A discussion on iterative methods, the construction of our preconditioner, and an introduction of the preconditioned F-GMRES method can be found in Section 3. Numerical results are presented in Section 4, and Section 5 contains concluding remarks.

2 Anti-reflective boundary conditions

We review some properties of blurring matrices with ARBCs. A survey of blurring matrices with ARBCs is given in [15], where many details are provided. Consider a blurring matrix A determined by a discretized PSF,

$$H = \begin{bmatrix} h_{-m,-m} & \cdots & & h_{-m,0} & & \cdots & h_{-m,m} \\ \vdots & \ddots & & \vdots & & & \vdots \\ & & h_{-1,-1} & h_{-1,0} & h_{-1,1} & & \\ h_{0,-m} & \cdots & h_{0,-1} & h_{0,0} & h_{0,1} & \cdots & h_{0,m} \\ & & h_{1,-1} & h_{1,0} & h_{1,1} & & \\ \vdots & & & \vdots & & \ddots & \vdots \\ h_{m,-m} & \cdots & & h_{m,0} & & \cdots & h_{m,m} \end{bmatrix} \in \mathbb{R}^{(2m+1)\times(2m+1)}, \quad (6)$$

with $h_{0,0}$ the central coefficient and, generally, $2m+1 \ll n$. The image values $f_{1-j,t}$ for $1 \le j \le m$ and $1 \le t \le n$ are represented by $2f_{1,t} - f_{j+1,t}$. Similarly, for $1 \le j \le m$ and $1 \le s,t \le n$, we obtain the image values

$$f_{s,1-j} = 2f_{s,1} - f_{s,j+1}, \quad f_{n+j,t} = 2f_{n,t} - f_{n-j,t}, \quad f_{s,n+j} = 2f_{s,n} - f_{s,n-j}.$$

When both indices of $f_{p,q}$ are outside the range $\{1,2,\ldots,n\}$, which happens for pixels close to the four corners of the given image, we carry out anti-reflection first in one space-direction (in the direction of the horizontal or vertical axis) and then in the other direction; see [13]. We describe these anti-reflections for pixels near

the corner with pixel index $(1,1)$ of an image; pixels near the other corners are treated analogously. Thus, for $1 \leq j,l \leq m$, we let

$$f_{1-j,1-l} = 4f_{1,1} - 2f_{1,l+1} - 2f_{j+1,1} + f_{j+1,l+1}.$$

Here we have carried out anti-reflection along the horizontal axis followed by anti-reflection along the vertical axis.

The strategy to anti-reflect first in one space-direction and then in an orthogonal space-direction yields a blurring matrix $A \in \mathbb{R}^{n^2 \times n^2}$ with a two-level structure; see [13]. Specifically, A is the sum of five matrices: A block Toeplitz matrix with Toeplitz blocks, a block Toeplitz matrix with Hankel blocks, a block Hankel matrix with Toeplitz blocks, a block Hankel matrix with Hankel blocks, and a matrix of rank at most $4n$. Despite this somewhat complicated structure, matrix-vector products with the matrix A can be evaluated in $\mathcal{O}(n^2 \log(n))$ arithmetic floating-point operations (flops) by applying the FFT as follows: Let the n^2-vectors $\boldsymbol{x} = X(:)$ and $\boldsymbol{y} = Y(:)$ be defined by stacking the columns of the $n \times n$-matrices X and Y, respectively. These matrices represent images; their entries are pixel values. For every kind of boundary conditions, the matrix-vector product $\boldsymbol{y} = A\boldsymbol{x}$ can be implemented by the following procedure:

1. pad X with the chosen boundary conditions obtaining an extended 2D array $\widetilde{X} \in \mathbb{R}^{(n+m)\times(n+m)}$;
2. compute $\widetilde{Y}$ as the circular convolution of $\widetilde{X}$ and H;
3. determine Y by extracting the central inner $n \times n$ part of $\widetilde{Y}$.

The anti-reflective boundary conditions require the use of an anti-symmetric pad analogous to the symmetric pad that is available for the MATLAB function padarray.[1] Further details are provided in [15].

3 The preconditioned iterative method

This section defines the preconditioners to be used and discusses the iterative solution of the preconditioned linear systems of algebraic equations (5) by the F-GMRES method.

3.1 Iterative regularization methods for anti-reflective boundary conditions

Introduce the correlation operator

$$[K^* f](\boldsymbol{x}) = \int_{\mathbb{R}^2} h(\boldsymbol{y} - \boldsymbol{x}) f(\boldsymbol{y}) \mathrm{d}\boldsymbol{y}, \tag{7}$$

which is the adjoint of the convolution operator in (1). Here we have used the fact that h is real-valued. Let the matrix A' be obtained by discretizing (7) with the same boundary conditions as for (3). It is proposed in [11] that, instead of solving (3), one should compute the solution of the linear system of equations

$$A'A\boldsymbol{f} = A'\boldsymbol{g} \tag{8}$$

[1] A MATLAB code for the anti-symmetric pad can be downloaded at
http://scienze-como.uninsubria.it/mdonatelli/Software/software.html

when RBCs or ARBCs are imposed and the PSF is quite general, such as a PSF that models motion blur. The linear system (8) is solved by a conjugate gradient (CG) method that is formally similar to the CGLS method [2]. The latter method computes an approximate solution of (3) by determining an approximate solution of the associated normal equations $A^TA\boldsymbol{f} = A^T\boldsymbol{g}$. It is suggested in [11] that the matrix A^T in the CGLS method be replaced by A'. Attractions of the so obtained iterative method for the approximate solution of (3) include that the matrix $A'A$ is not explicitly formed (only matrix vector products with the matrices A and A' are evaluated) and that the method uses short recurrence relations. Therefore, the method requires fairly little computer storage. The reason for using A' instead of A^T in (8) is that the evaluation of matrix-vector products with the latter matrix is more cumbersome and may suffer from numerical instability; see, e.g., [14] for a recent discussion.

However, the iterative solution of (8) by the CG method is not without difficulties. The main problem is that the matrix $A'A$ is not symmetric positive definite and, therefore, the application of the CG method to the solution of (8) has no theoretical justification. Moreover, the computed restorations may be of poor quality, in particular when the PSF is strongly non-symmetric; see the analysis in [14]. These difficulties with the CG method prompted the investigation in [14] of the application of GMRES-type methods to the solution of (8).

GMRES is an iterative method proposed in [32] for the solution of linear systems of algebraic equations with a fairly general square non-symmetric non-singular matrix; see also [31]. Among several solution methods investigated in [14], the application of GMRES to the system

$$AA'\boldsymbol{z} = \boldsymbol{g} \tag{9}$$

performed the best. When $\boldsymbol{z}$ is an approximate solution of (9), $\boldsymbol{f} = A'\boldsymbol{z}$ is an approximate solution of (3). We may consider A' a right preconditioner. Right-preconditioning is convenient to use when the number of iterations is determined with the aid of the discrepancy principle; see below. We next describe several preconditioners.

To justify the definition of our preconditioner, we first discuss left-preconditioned Landweber iteration. Following [7], where the so called "Z variant" is described, we consider the left-preconditioned system

$$ZA\boldsymbol{f} = Z\boldsymbol{g} \tag{10}$$

obtained from (3). Application of Landweber iteration to the solution of (10) yields the iterates

$$\boldsymbol{f}_{k+1} = \boldsymbol{f}_k + Z(\boldsymbol{g} - A\boldsymbol{f}_k). \tag{11}$$

We may determine the preconditioner $Z \in \mathbb{R}^{n^2\times n^2}$ by filtering as follows: In the case of PBCs, A is a BCCB matrix, which can be diagonalized by the 2D discrete Fourier transform. The eigenvalues $\lambda_{i,j}$ of A, for $i,j = 0,\ldots,n-1$, can be computed by the 2D FFT applied to its first column arranged as a 2D array. The matrix Z is chosen to be a BCCB matrix, whose eigenvalues $\breve{\lambda}_{i,j}$ are obtained by applying some filter to the $\lambda_{i,j}$. For instance, we may use a slightly modified version of the Tikhonov filter

$$\breve{\lambda}_{i,j} = \frac{\overline{\lambda}_{i,j}}{\left|\lambda_{i,j}\right|^2 + \alpha}, \qquad i,j = 0,1,\ldots,n-1,$$

where $\alpha > 0$ is a regularization parameter and the bar denotes complex conjugation. The BCCB matrix Z can be defined analogously for other boundary conditions; see [7] for details.

When applying a stationary preconditioned iterative regularization method, we have to face the non-trivial task of determining a suitable value of the parameter α. A too small value of α often gives fast convergence, but may cause instability due to severe ill-conditioning of the preconditioner. The instability may result in large propagated errors, which may reduce the quality of the computed solution and possibly make the computed solution useless. On the other hand, a too large value of α may result in slow convergence of the computed iterates. Hence, a proper choice of α is important. Since iterative regularization methods are filtering methods, and the filter changes with the iteration number, it can be difficult to determine a priori a value of α that is suitable for all iterations. Here we also note that the number of iterations required is typically not known before the iterative solution process is started.

To avoid the task of determining a suitable value of α before the start of the iterations, Donatelli and Hanke [12] proposed the following non-stationary version of the iterations (11),

$$\boldsymbol{f}_{k+1} = \boldsymbol{f}_k + Z^k_{\text{circ}}\boldsymbol{r}_k, \quad Z^k_{\text{circ}} = C^T(CC^T + \alpha_k I)^{-1}, \quad \boldsymbol{r}_k = \boldsymbol{g} - A\boldsymbol{f}_k. \tag{12}$$

Here C is the BCCB matrix associated with the PSF that defines the matrix A in (3) and α_k is determined by solving a non-linear equation by Newton's method; see [12] for details.

Recently, Dell'Acqua et al. [8] extended the non-stationary method (12) to be able to take the boundary conditions of the problem into account and proposed the following iteration scheme,

$$\boldsymbol{f}_{k+1} = \boldsymbol{f}_k + Z^k_{\text{struct}}\boldsymbol{r}_k, \quad Z^k_{\text{struct}} = \mathcal{B}(C^T(CC^T + \alpha_k I)^{-1}), \quad \boldsymbol{r}_k = \boldsymbol{g} - A\boldsymbol{f}_k, \tag{13}$$

where the operator $\mathcal{B}$ denotes the application of boundary conditions to the circulant matrix $C^T(CC^T + \alpha_k I)^{-1}$. Thus, the operator $\mathcal{B}$ affects the structure of the matrix Z^k_{struct}.

The matrix Z^k_{struct} may be considered a preconditioner. In particular, we may solve the right-preconditioned linear system (5) with the preconditioner

$$P_k = \mathcal{B}(C^T(CC^T + \alpha_k I)^{-1}) \tag{14}$$

by F-GMRES. The parameter α_k allows the preconditioner P_k to be varied during the iterations.

Note that the preconditioner (14) is not explicitly formed, only matrix-vector products with P_k are computed. Indeed, the matrix C is not explicitly formed; instead matrix-vector products are evaluated by circular convolutions with the coefficient mask H, i.e., with the PSF. The same can be done for Z^k_{circ} and Z^k_{struct}. We remark that the structure of Z^k_{struct} may be quite involved depending on the boundary conditions, but, using the procedure described at the end of Section 2, only a 2D coefficient mask $\breve{H}$ is required to be used instead of H. The procedure for computing $\breve{H}$ is described in the next subsection.

3.2 Construction of the preconditioners

The generating function associated with the PSF defined by H in (6) is given by

$$f(x_1, x_2) = \sum_{j_1=-m}^{m} \sum_{j_2=-m}^{m} h_{j_1,j_2} \mathrm{e}^{\hat{\imath}(j_1 x_1 + j_2 x_2)}, \qquad \hat{\imath} = \sqrt{-1}. \tag{15}$$

Thus, the entries h_{j_1,j_2} of the matrix H are Fourier coefficients of the function f.

Let $y_k^{(n)} = 2\pi k/n$, for $k = 0, \ldots, n-1$, be a uniform sampling on the interval $[0, 2\pi]$. The 2D Fourier matrix of order $n^2 \times n^2$ is given by

$$F_{(n,n)} = F_n \otimes F_n, \quad \text{where} \quad F_n = \frac{1}{\sqrt{n}} \left[\mathrm{e}^{-\hat{\imath} j y_k^{(n)}} \right]_{k,j=0}^{n-1}$$

and $\otimes$ denotes the Kronecker product. Given the function f in (15), the BCCB matrix C generated by f is defined as

$$C = \mathcal{C}_{(n,n)}(f) = F_{(n,n)} D_{(n,n)}(\lambda) F_{(n,n)}^H,$$

where $D_{(n,n)}(\lambda) = \mathrm{diag}_{i,j=0,\ldots,n-1}[\lambda_{i,j}]$ is the diagonal matrix of its eigenvalues and $F_{(n,n)}^H$ is the conjugate transpose of $F_{(n,n)}$. The eigenvalues $\lambda_{i,j}$, $0 \le i, j < n$, of C are determined by a uniform sampling of the generating function f in (15) at the grid points $\Gamma_n = \{(y_i^{(n)}, y_j^{(n)}) \,:\, i, j = 0, 1, \ldots, n-1\}$, namely

$$\lambda_{i,j} = f\left(\frac{2\pi i}{n}, \frac{2\pi j}{n} \right), \qquad i, j = 0, 1, \ldots, n-1. \tag{16}$$

Therefore, the PSF can be interpreted as a mask of Fourier coefficients, and the BCCB matrix C generated by f in (15) coincides with the matrix A in (3) when PBCs are imposed.

The preconditioner is constructed by using the Tikhonov filter, but other filters can be applied as well. The Tikhonov solution of the linear system $C\boldsymbol{f} = \boldsymbol{g}$ is

$$\boldsymbol{f}_\alpha = (C^T C + \alpha I)^{-1} C^T \boldsymbol{g} = C^T (C C^T + \alpha I)^{-1} \boldsymbol{g}.$$

The BCCB matrix $C^T (C C^T + \alpha I)^{-1}$ has the eigenvalues

$$\breve{\lambda}_{i,j} = \frac{\overline{\lambda}_{i,j}}{|\lambda_{i,j}|^2 + \alpha} = \frac{\overline{f}(\frac{2\pi i}{n}, \frac{2\pi j}{n})}{|f(\frac{2\pi i}{n}, \frac{2\pi j}{n})|^2 + \alpha}, \qquad i, j = 0, 1, \ldots, n-1. \tag{17}$$

Similarly to (16), assuming for simplicity that n is odd, the eigenvalues $\breve{\lambda}_{i,j}$ may be considered a sampling of the function

$$g(x_1, x_2) = \sum_{j_1, j_2 = -\frac{n-1}{2}}^{\frac{n-1}{2}} \beta_{j_1,j_2} \mathrm{e}^{\hat{\imath}(j_1 x_1 + j_2 x_2)}$$

at the grid points Γ_n for the specific choice of the coefficients β_{j_1,j_2} as now discussed. The trigonometric polynomial g is determined by the n^2 interpolation conditions $\breve{\lambda}_{i,j} := g\left(\frac{2\pi i}{n}, \frac{2\pi j}{n} \right)$ and its coefficients β_{j_1,j_2} can be computed by means of a two-dimensional IFFT. Note that g is a regularized approximation of the inverse of f on Γ_n. Let $\breve{H}$ denote the mask for the Fourier coefficients β_{j_1,j_2}. It can be determined by carrying out the following steps:

1. Compute $\lambda_{i,j}$ in (16) by the FFT applied to H.
2. Compute $\breve{\lambda}_{i,j}$ in (17).
3. Compute $\breve{H}$ by the IFFT applied to $\breve{\lambda}_{i,j}$.

In actual computations, we modify the BCCB matrix $C^T(CC^T + \alpha I)^{-1}$ to correspond to ARBCs. This yields a structured preconditioner $P = \mathcal{B}(C^T(CC^T + \alpha I)^{-1})$, where $\mathcal{B}$ is an operator that imposes the ARBCs. As already mentioned at the end of Section 2, the matrix P is not explicitly formed, but only $\breve{H}$ is stored and a matrix-vector product with P is evaluated in $\mathcal{O}(n^2 \log(n))$ flops by using the anti-symmetric pad and convolution with $\breve{H}$.

3.3 The flexible GMRES method

The F-GMRES method [30] is a minimal residual iterative method that is designed for application of a sequence of preconditioners. We will use F-GMRES with preconditioners of the form (14) that are determined by a sequence of α_k-values.

Given a set of ℓ linearly independent vectors $\boldsymbol{u}_1, \boldsymbol{u}_2, \ldots, \boldsymbol{u}_\ell \in \mathbb{R}^{n^2}$, the F-GMRES method determines a decomposition of the form

$$AU_\ell = V_{\ell+1} H_{\ell+1,\ell}, \tag{18}$$

where $U_\ell = [\boldsymbol{u}_1, \boldsymbol{u}_2, \ldots, \boldsymbol{u}_\ell] \in \mathbb{R}^{n^2 \times \ell}$, $V_{\ell+1} = [\boldsymbol{v}_1, \boldsymbol{v}_2, \ldots, \boldsymbol{v}_{\ell+1}] \in \mathbb{R}^{n^2 \times (\ell+1)}$ has orthonormal columns with $\boldsymbol{v}_1 = \boldsymbol{g}/\|\boldsymbol{g}\|$, and $H_{\ell+1,\ell} = [h_{i,j}] \in \mathbb{R}^{(\ell+1)\times \ell}$ is of upper Hessenberg type. Let $\boldsymbol{e}_1 = [1, 0, \ldots, 0]^T \in \mathbb{R}^{\ell+1}$ denote the first axis vector. Then

$$\min_{\boldsymbol{w} \in \mathrm{range}(U_\ell)} \|A\boldsymbol{w} - \boldsymbol{g}\| = \min_{\boldsymbol{y} \in \mathbb{R}^\ell} \|AU_\ell \boldsymbol{y} - \boldsymbol{g}\| = \min_{\boldsymbol{y} \in \mathbb{R}^\ell} \|H_{\ell+1,\ell}\boldsymbol{y} - \boldsymbol{e}_1 \|\boldsymbol{g}\| \|, \tag{19}$$

where $\|\cdot\|$ denotes the Euclidean vector norm.

Assume that the matrix $H_{\ell+1,\ell}$ exists and that all its subdiagonal entries are positive. This is the generic situation. The positivity of the subdiagonal entries of the upper Hessenberg matrix $H_{\ell+1,\ell}$ secures that its columns are linearly independent. We remark that the parameter ℓ in (18) generally is fairly small in our applications.

The minimization problem on the right-hand side of (19) has a unique solution $\boldsymbol{y}_\ell \in \mathbb{R}^\ell$, which determines the approximate solution $\boldsymbol{f}_\ell = U_\ell \boldsymbol{y}_\ell$ of (3). Since ℓ is small, the solution $\boldsymbol{y}_\ell$ easily can be computed by QR factorization of the matrix $H_{\ell+1,\ell}$. In our application of the decomposition (18), the vectors $\boldsymbol{u}_k$ are determined with the preconditioners P_k; see (14) and Algorithm 1 below. A discussion on the choice of the parameters α_k in the preconditioner P_k and on the choice of ℓ in (18) is provided in Subsection 3.4.

Algorithm 1 *The F-GMRES method*
1. $\boldsymbol{v}_1 = \boldsymbol{g}/\|\boldsymbol{g}\|$
2. for $k = 1, 2, \ldots, \ell$ *do*
3. $\quad \boldsymbol{u}_k = P_k \boldsymbol{v}_k$*;* $\boldsymbol{v} = A\boldsymbol{u}_k$
4. $\quad$ *for* $i = 1, 2, \ldots, k$ *do*
5. $\quad\quad h_{i,k} = \boldsymbol{v}^T \boldsymbol{v}_i$*;* $\boldsymbol{v} = \boldsymbol{v} - h_{i,k}\boldsymbol{v}_i$
6. $\quad$ *end*
7. $\quad h_{k+1,k} = \|\boldsymbol{v}\|$*;* $\boldsymbol{v}_{k+1} = \boldsymbol{v}/h_{k+1,k}$

8. end
9. define $U_\ell = [\boldsymbol{u}_1, \boldsymbol{u}_2, \ldots, \boldsymbol{u}_\ell] \in \mathbb{R}^{n^2 \times \ell}$ *and* $H_{\ell+1,\ell} = [h_{i,j}] \in \mathbb{R}^{(\ell+1)\times\ell}$ *upper Hessenberg*
10. compute $\boldsymbol{y}_\ell := \arg\min_{\boldsymbol{y}\in\mathbb{R}^\ell} \|H_{\ell+1,\ell}\boldsymbol{y} - \boldsymbol{e}_1\|\boldsymbol{g}\|\|$ *and* $\boldsymbol{f}_\ell = U_\ell \boldsymbol{y}_\ell$

We say that F-GMRES breaks down at step k if $h_{k+1,k} = 0$ and $h_{j+1,j} > 0$ for $1 \leq j < k$. As already mentioned, this is a rare event. Discussions on breakdown of F-GMRES can be found in [27,30].

Algorithm 1 requires that both the matrix $V_{\ell+1}$ and the vectors $\boldsymbol{u}_k = P_k \boldsymbol{v}_k$, $1 \leq k \leq \ell$, be stored. This implies that F-GMRES demands more storage space than (standard) GMRES after the same number of steps, since GMRES only requires storage of the matrix $V_{\ell+1}$. However, the fact that F-GMRES allows non-stationary preconditioning, while GMRES does not, may be worth the extra storage cost. Note that if we let $P_k = P$ be independent of k, then Algorithm 1 can be replaced by the preconditioned (standard) GMRES method; see [31] for a discussion of the latter.

A difference between the F-GMRES and GMRES algorithms is that the action of AP_k on a vector $\boldsymbol{v}$ generally is not in the range of $V_{\ell+1}$ in F-GMRES. Instead, we have the following result, which is a consequence of (19).

Proposition 1 *The approximate solution* $\boldsymbol{f}_\ell$ *obtained at step* ℓ *of F-GMRES minimizes the residual norm* $\|\boldsymbol{g} - A\boldsymbol{f}_\ell\|$ *over* $\mathrm{range}(U_\ell)$.

Another difference is that, while for standard GMRES with initial iterate in $\mathrm{span}\{\boldsymbol{g}\}$ breakdown is equivalent to convergence, this is not the case for F-GMRES. Moreover, it is difficult to show convergence results for F-GMRES since, differently from standard GMRES, there is no isomorphism between the solution subspace of F-GMRES and the space of polynomials. For more information, we refer to [27, 30,31].

3.4 The stopping criterion and the choice of regularization parameters

This subsection discusses how to determine the number of iterations, ℓ, with Algorithm 1 and how to choose the parameters α_k of the preconditioners P_k; see (14). We will assume that a fairly accurate bound ε for the norm of the error $\boldsymbol{\nu}$ in the vector $\boldsymbol{g}$ is available. Thus,

$$\|\boldsymbol{\nu}\| \leq \varepsilon.$$

Let $\boldsymbol{f}_1, \boldsymbol{f}_2, \boldsymbol{f}_3, \ldots$ be a sequence of approximate solutions of (3) determined by Algorithm 1 and define the associated residual vectors $\boldsymbol{r}_\ell = \boldsymbol{g} - A\boldsymbol{f}_\ell$, $\ell = 1, 2, 3, \ldots$. The discrepancy principle prescribes that the iterations with Algorithm 1 be terminated as soon as a residual vector $\boldsymbol{r}_\ell$ that satisfies

$$\|\boldsymbol{r}_\ell\| \leq \eta\varepsilon \tag{20}$$

has been determined, where $\eta \geq 1$ is a user-specified constant independent of ε. We set $\eta = 1$ in the computed examples reported in Section 4. This stopping criterion is reasonable, because the desired exact solution $\boldsymbol{f}$ satisfies $\|A\boldsymbol{f} - \boldsymbol{g}\| = \|\boldsymbol{\nu}\|$. Note that since

$$\|\boldsymbol{r}_\ell\| = \|H_{\ell+1,\ell}\boldsymbol{y}_\ell - \boldsymbol{e}_1\|\boldsymbol{g}\|\|,$$

we can check whether (20) holds without explicitly forming the residual vector $\boldsymbol{r}_\ell$.

We use a progressive implementation of F-GMRES in the computed examples. This implementation updates the matrix $H_{\ell+1,\ell}$ for $\ell = 1, 2, 3, \ldots$ together with its QR factorization. The solution $\boldsymbol{y}_\ell$ of the small least-squares problem in the right-hand side of (19) is computed for every ℓ. This makes it easy to determine when (20) holds for the first time and, therefore, when the iterations should be terminated.

We now describe the determination of the parameters α_k of the preconditioners P_k, $k = 1, 2, 3, \ldots$. A well-established choice of the regularization parameter in the context of iterated Tikhonov methods is the geometric sequence

$$\alpha_k = \alpha_0 q^{k-1}, \qquad k = 1, 2, 3, \ldots , \tag{21}$$

where $\alpha_0 > 0$ and $0 < q < 1$; see, e.g., [3,12]. This choice also is used for Bregman iteration [4,26]. The value of the initial regularization parameter α_0 is not critical as long as it is not too small.

A different technique to determine the regularization parameter α_k is described in [12]: At step k the parameter α_k is determined by solving the non-linear equation

$$\|\boldsymbol{r}_k - C Z_{\text{circ}}^k \boldsymbol{r}_k\| \;=\; q_k \|\boldsymbol{r}_k\| \tag{22}$$

with a few steps of Newton's method, where

$$q_k = \max\{q,\, 2\rho_{\text{circ}} + (1 + \rho_{\text{circ}})\delta / \|\boldsymbol{r}_k\|\} \tag{23}$$

and Z_{circ}^k is defined as in (12). The parameter q is included in (23) as a safeguard to prevent that the q_k decrease too rapidly with increasing k. We remark that the theoretical results in [12] do not use the parameters q in (23). The parameter $0 < \rho_{\text{circ}} < 1/2$ should be as small as possible and satisfy

$$\|(C - A)\boldsymbol{z}\| \;\leq\; \rho_{\text{circ}} \, \|A\boldsymbol{z}\| , \qquad \forall\, \boldsymbol{z} \in \mathbb{R}^n . \tag{24}$$

If A is accurately approximated by its BCCB counterpart C, then this inequality can be approximately satisfied for a small value of ρ_{circ}. This parameter has to be set in the algorithm described in [12]; for image deblurring problems, it is usually chosen as 10^{-2} or 10^{-3}. A too small value of ρ_{circ} can easily be recognized by an oscillatory behavior of the α_k with increasing values of k; see [12].

In [8], the same approach is applied to the structured case. The goal is to estimate α_k by solving

$$\|\boldsymbol{r}_k - A Z_{\text{struct}}^k \boldsymbol{r}_k\| \;=\; q_k \|\boldsymbol{r}_k\| \tag{25}$$

for α_k defining Z_{struct}^k as described by (13). This is not computationally practicable when the PSF has a non-symmetric structure. Instead, the regularization parameter α_k is estimated by using equation (22), which may be considered a computable approximation of (25). Note that even though we again use equation (22) to estimate the parameters α_k, we obtain a different parameter sequence $\alpha_1, \alpha_2, \alpha_3, \ldots$, because the sequence of residual vectors differs. Furthermore, in this case condition (24) is not meaningful. Therefore, a new parameter ρ_{struct} is introduced and the iterations are terminated by the discrepancy principle (20) with

$$\eta = \frac{1 + 2\rho_{\text{struct}}}{1 - 2\rho_{\text{struct}}}. \tag{26}$$

In the following, we refer to the sequence $\alpha_1, \alpha_2, \alpha_3, \dots$ computed in the way described as the DH sequence, since it is a development of an idea introduced in [12]. We set $q = 0.8$ and $\rho_{\text{struct}} = 10^{-2}$ in all the computed examples.

We turn to a new technique for determining the parameters α_k. Assume that

$$\|\boldsymbol{r}_k\| = c_k \alpha_k^p,$$

where $c_k > 0$ and α_k are positive scalars, and $p \geq 1$ is a fixed exponent. Requiring that $\|\boldsymbol{r}_k\| = \varepsilon$ yields

$$\alpha_k = \sqrt[p]{\frac{\varepsilon}{c_k}}.$$

Assuming that

$$c_k \approx c_{k-1} = \frac{\|\boldsymbol{r}_{k-1}\|}{\alpha_{k-1}^p},$$

we obtain the sequence

$$\begin{aligned} \alpha_1 &= \alpha_0, \\ \alpha_k &= \sqrt[p]{\frac{\varepsilon}{\|\boldsymbol{r}_{k-1}\|}}\, \alpha_{k-1}, \qquad k = 2, 3, \dots , \end{aligned} \tag{27}$$

where $\alpha_0 > 0$. In other words, the update from α_{k-1} to α_k is based on the ratio of the error bound ε and the norm of the residual relative to the previous iteration. The heuristic motivation behind this strategy is that α_k is computed in order to make the norm of the residual $\|\boldsymbol{r}_k\|$ move towards ε as k increases. When using (27), the key parameter for the generation of the sequence $\{\alpha_k\}$ is p. In the computed examples, we set $\alpha_0 = 1$ and we illustrate that $p = 2$ is a good choice for all the considered examples.

4 Numerical results

This section reports some numerical results that show the performance of the methods described. We consider two deblurring problems with non-symmetric PSFs and low noise levels, and apply ARBCs. It is the purpose of the examples to illustrate the efficacy of non-stationary structure-preserving preconditioners for F-GMRES and Landweber iteration. The use of different techniques for computing the sequence of regularization parameters is illustrated.

4.1 Test problems

Figure 1 displays images for our first test problem (Test 1). The left panel shows the uncontaminated (exact) camera man image. We take a larger image and crop it (see the white box in Figure 1(a)). The image inside the box is made up of 227×227 pixels and is assumed not to be available. The PSF, which is three quarters of a Gaussian blur, is shown in the middle panel of Figure 1. It is made up of 29×29 pixels. The (available) blur- and noise-contaminated image is displayed by the right panel of Figure 1. It is computed by applying the PSF to the larger image

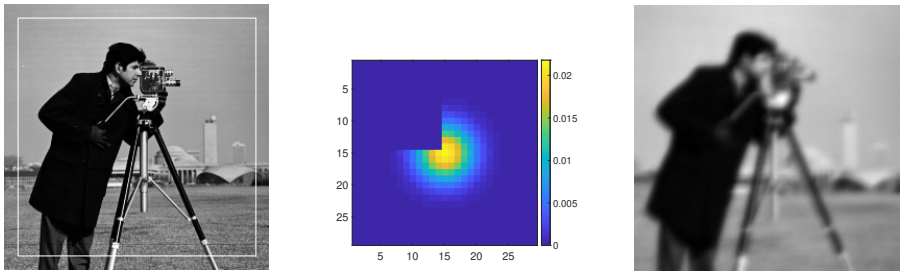

(a) (b) (c)

Fig. 1 [Test 1] (a) True image, (b) PSF, (c) blurred and noisy image.

of the left panel, adding 0.5% white Gaussian noise, and then using a 227×227 pixel subimage.

Let the vector $\boldsymbol{f} \in \mathbb{R}^{227^2}$ represent the desired uncontaminated image, where we order the pixels of the image column-wise. Similarly, we let the vector $\boldsymbol{f}_{\text{restored}} \in \mathbb{R}^{227^2}$ represent the restored image determined by one of the methods in our comparison. We refer to

$$\frac{\|\boldsymbol{f}_{\text{restored}} - \boldsymbol{f}\|}{\|\boldsymbol{f}\|}$$

as the relative restoration error (RRE).

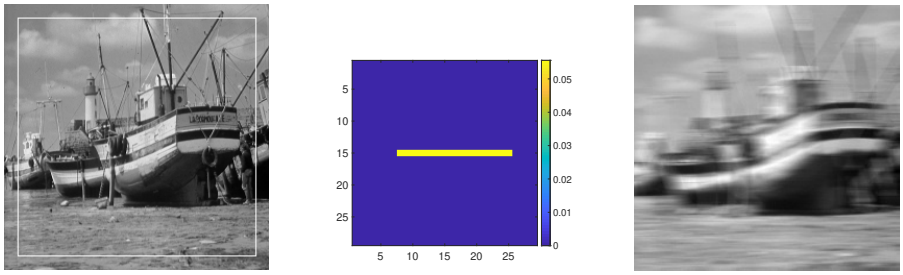

(a) (b) (c)

Fig. 2 [Test 2] (a) True image, (b) PSF, (c) blurred and noisy image.

Figure 2 shows images for our second test problem (Test 2), and is analogous to Figure 1. The uncontaminated unavailable (exact) boat image is made up of 227×227 pixels and shown inside the white box of Figure 2(a). The middle panel depicts the non-symmetric PSF. It models motion blur and is made up of 29×29 pixels. The right panel displays the available blur- and noise-contaminated image. The noise is 0.6% white Gaussian.

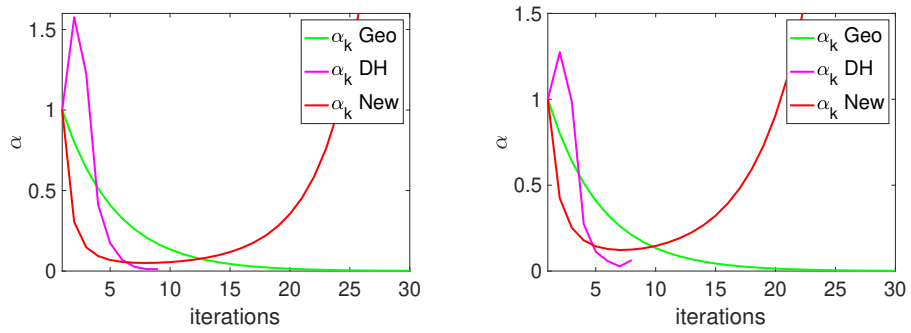

Fig. 3 Plots of the α_k as a function of k related to F-GMRES for the geometric sequence, the DH sequence, and the new sequence for Test 1 (on the left) and Test 2 (on the right).

4.2 Restorations, plots, and tables

We compare the unpreconditioned CGLS and GMRES methods to non-stationary preconditioned F-GMRES. Throughout this section CGLS refers to the conjugate gradient method applied to the solution of the linear system of equations (8); see the discussion in Subsection 3.1. Also preconditioned Landweber as described in [8] is considered. The preconditioners are determined by the regularization parameters α_k defined by (21), (22), or (27). We refer to these sequences of regularization parameters as the "geometric sequence", the "DH sequence", and the "new sequence", respectively. We always set $\alpha_0 = 1$ and let $q = 0.8$ for the geometric sequence, $q = 0.8$ and $\rho_{\text{struct}} = 10^{-2}$ for the DH sequence, and $p = 2$ for the new sequence. These three approaches to choosing the α_k are used for both the Z^k_{struct}-Landweber and F-GMRES iterations. Figure 3 shows the α_k for F-GMRES. It can be seen that these three approaches give quite different parameter sequences $\alpha_1, \alpha_2, \alpha_3, \ldots$; the geometric sequence converges to zero at a rate that depends on the choice of q; the DH sequence achieves values larger than unity in the first steps, and then the sequence decreases rapidly. Finally, the sequence (27) decreases quickly to a small value (close to 0) and then increases.

Figures 4 and 5 show (for Test 1 and Test 2, respectively) restorations determined by different methods when the iterations are terminated by the discrepancy principle using (20), and when applicable (26), and the α_k are determined as described in [12]. The restored images look essentially the same; also their RRE values are close. The non-stationary preconditioners of this paper give rapid convergence and restorations of high quality. Tables 1 and 2 report (for Test 1 and Test 2, respectively) the RRE and the number of iterations (IT) required to achieve the best restoration (i.e., the restoration with the smallest RRE) and the restoration determined with the discrepancy principle. The symbol — in the tables indicates that the discrepancy principle cannot be satisfied, while the symbol n/a means that no meaningful best restoration is available. This situation may arise when the method [12] is applied, because the iterations with this method terminate with the discrepancy principle.

Figures 6 and 7 show (for Test 1 and Test 2, respectively) the RRE as a function of the iteration number. Solid curves are used for CGLS, GMRES, and

(a) (b) (c)

Fig. 4 [Test 1] Restorations determined with the discrepancy principle by (a) CGLS (RRE 0.0923, IT 27); (b) F-GMRES New (RRE 0.0907, IT 8); (c) Z^k_{struct}-Landweber New (RRE 0.0942, IT 12).

(a) (b) (c)

Fig. 5 [Test 2] Restorations determined with the discrepancy principle by (a) CGLS (RRE 0.0948, IT 17); (b) F-GMRES DH (RRE 0.0925, IT 7); (c) Z^k_{struct}-Landweber DH (RRE 0.0917, IT 12).

F-GMRES, while dashed curves are used for Z^k_{struct}-Landweber. For the F-GMRES and Z^k_{struct}-Landweber plots, we use colors to show how the parameter values for the non-stationary preconditioners are determined. The iteration associated with the best restoration is marked by the symbol $\circ$, while the iteration identified by the discrepancy principle is marked by the symbol $\times$. Note that for the proposed F-GMRES, the discrepancy principle works very well. The maximum number of iterations is set to 100.

Method	RRE best res.	IT	RRE discrepancy	IT
CGLS	0.0895	36	0.0923	27
GMRES	0.1470	5	—	—
F-GMRES Geo	0.0897	13	0.0908	12
F-GMRES DH	n/a	n/a	0.0905	8
F-GMRES New	0.0898	9	0.0907	8
Z^k_{struct}-Landweber Geo	0.0889	23	0.0941	20
Z^k_{struct}-Landweber DH	n/a	n/a	0.0954	13
Z^k_{struct}-Landweber New	0.0888	18	0.0942	12

Table 1 [Test 1] Relative restoration error (RRE) and iteration number (IT) for the best restoration and when using the discrepancy principle for different methods.

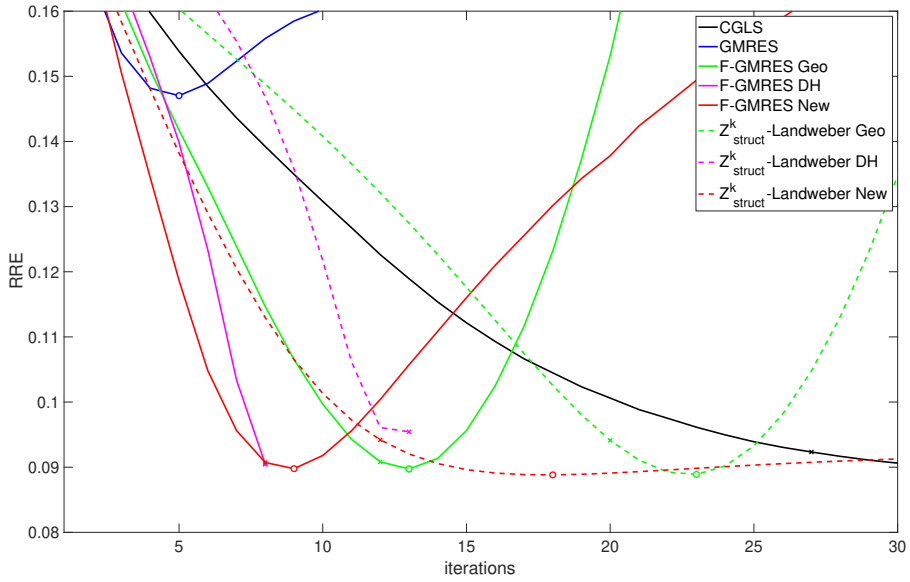

Fig. 6 [Test 1] Plots of the RRE for different methods. The iterate that gives the best restoration is marked by ∘, and the iterate determined by the discrepancy principle is marked by ×.

Method	RRE best res.	IT	RRE discrepancy	IT
CGLS	0.0939	15	0.0948	17
GMRES	0.1072	84	—	—
F-GMRES Geo	0.0931	8	0.0935	9
F-GMRES DH	n/a	n/a	0.0925	7
F-GMRES New	0.0932	7	0.0932	7
Z^k_{struct}-Landweber Geo	0.0912	17	—	—
Z^k_{struct}-Landweber DH	n/a	n/a	0.0917	12
Z^k_{struct}-Landweber New	0.0912	12	0.0917	13

Table 2 [Test 2] Relative restoration error (RRE) and iteration number (IT) for the best restoration and for the iterate determined by the discrepancy principle for different methods.

Standard GMRES can be seen to perform poorly for both image restoration problems. The best restoration determined by GMRES has a larger error than the best restoration achieved with any of the other methods in our comparison. Moreover, the discrepancy principle fails to terminate the iterations within 100 steps. Discussions on why GMRES may perform poorly for some restoration problems can be found in [14, 20].

The restorations computed by CGLS are quite accurate, in particular for Test 1. However, CGLS requires a large number of iterations in comparison to the other methods considered, where we recall that each iteration with CGLS demands two matrix-vector product evaluations, one with A and one with A'.

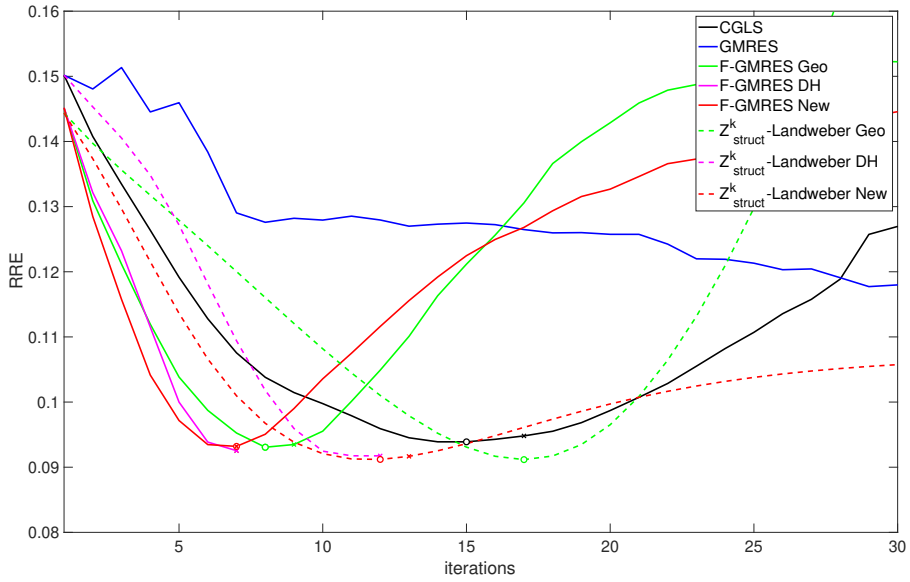

Fig. 7 [Test 2] Plots of RRE for different methods. The iterate that gives the best restoration is marked by ∘, and the iterate determined by the discrepancy principle is marked by ×.

Comparing the preconditioned F-GMRES method to the Z^k_{struct}-Landweber method described in [8], we note that the latter usually achieves an insignificantly smaller RRE, but preconditioned F-GMRES requires fewer iterations and terminates reliably with the aid of the discrepancy principle. Note that in Test 2, the discrepancy principle fails to terminate the iterations with Z^k_{struct}-Landweber Geo.

In summary, the non-stationary preconditioning approach can be used effectively with F-GMRES. Comparing the different ways to determine the parameters α_k for the preconditioners, Figures 6 and 7 show the sequence (27) to give the fastest convergence in both Test 1 and Test 2 for both the F-GMRES and Z^k_{struct}-Landweber methods.

4.3 Robustness analysis of P-GMRES

To better justify the non-stationary preconditioning approach of this paper, we present some numerical results for P-GMRES, i.e., GMRES with the same preconditioner for all iterations; all α_k have the same value α in each step. We illustrate that differently from F-GMRES with the different preconditioning strategies previously described, P-GMRES is very sensitive to the choice of α.

Figure 8 displays how α affects the number of iterations required to satisfy the discrepancy principle and to determine the best restoration. We can see that more iterations are required for larger values of α. Moreover, Figure 8 shows that termination of the iterations with the discrepancy principle does not work well when α is too small. In fact, the number of iterations grows in Test 1 when α is

reduced, while in Test 2 the discrepancy principle fails to stop the iterative method for α smaller than 10^{-2}.

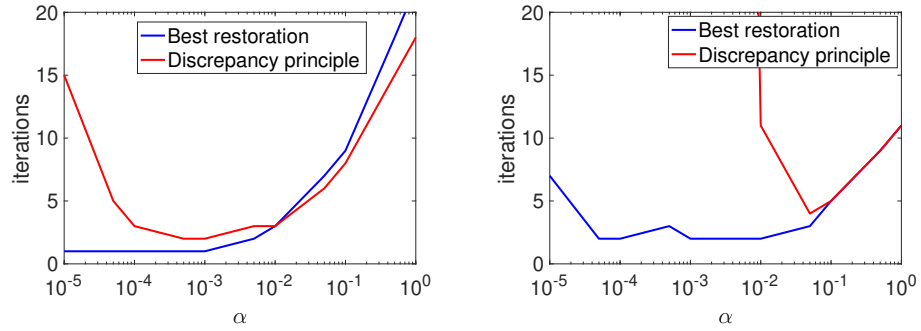

Fig. 8 Plot of the number of iterations with P-GMRES that gives the best restorations as a function of α (blue curve), and plot of the number of iterations with P-GMRES determined by the discrepancy principle as a function of α (red curve) for Test 1 (on the left) and for Test 2 (on the right).

The quality of the computed restorations is depicted in Figure 9. The blue curves show the RRE for the best restorations determined by P-GMRES for different values of α. The red curves show the RRE when terminating the iterations with the discrepancy principle. When α is reduced, the quality of restorations quickly deteriorates. We can notice again that the discrepancy principle does not work well; in Test 2 it is not able to stop the method for α smaller than 10^{-2}.

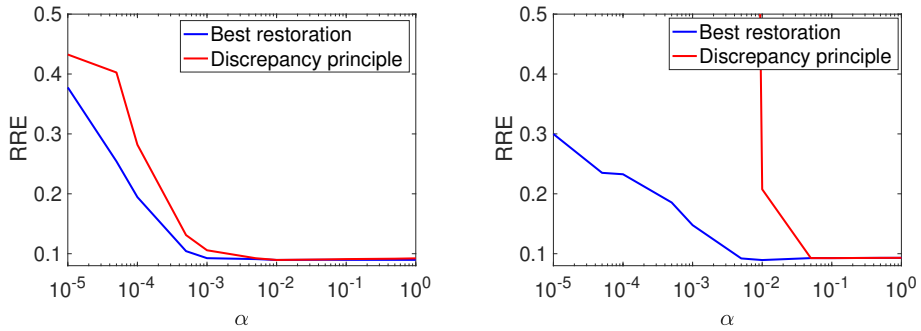

Fig. 9 Plot of the RRE for the best restoration computed by P-GMRES as a function of α (blue curve) and plot of the RRE for the P-GMRES iterate determined by the discrepancy principle as a function of α (red curve) for Test 1 (on the left) and for Test 2 (on the right).

4.4 Robustness analysis of the DH sequence

The DH sequence depends on the choice of parameters q and ρ_{struct}. The former parameter is included as a safeguard to prevent the q_k in (22) from decreasing too rapidly. We set $q = 0.8$, the same as for the geometric sequence. This subsection shows the robustness of F-GMRES with respect to the choice of ρ_{struct}.

Figure 10 displays how ρ_{struct} affects the number of iterations required to satisfy the discrepancy principle. As expected, we can see that fewer iterations are required for larger values of ρ_{struct}.

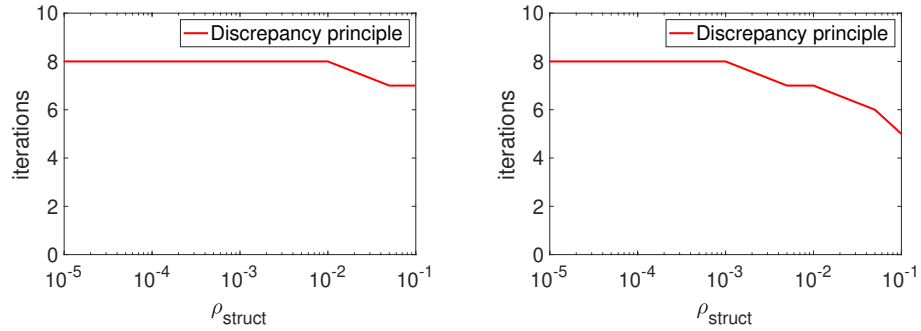

Fig. 10 Plots of the number of iterations by F-GMRES DH determined by the discrepancy principle as a function of ρ_{struct} for Test 1 (on the left) and for Test 2 (on the right).

The quality of the computed restorations is depicted in Figure 11. The curves show the RRE when terminating the iterations with the discrepancy principle. We can notice a stable behavior when ρ_{struct} decreases. For Test 1, $\rho \in [10^{-5}, 10^{-2}]$ gives exactly the same results in terms of RRE and number of iterations. Similarly, for Test 2 the results are not sensitive to a decease in ρ. Therefore, a careful tuning of the parameters ρ and ρ_{struct} is not required when using F-GMRES.

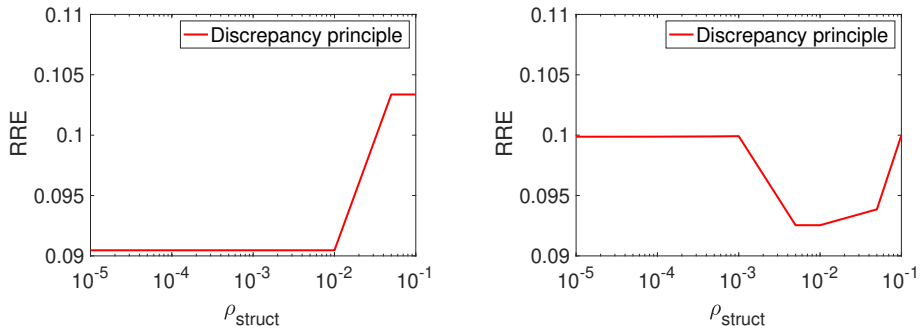

Fig. 11 Plots of the RRE for iterates computed by F-GMRES DH using the discrepancy principle as a function of ρ_{struct} for Test 1 (on the left) and for Test 2 (on the right).

4.5 Robustness analysis of the new sequence

The sequence (27) depends on the choice of the parameter p. This subsection seeks to shed light on how this choice affects the performance of F-GMRES.

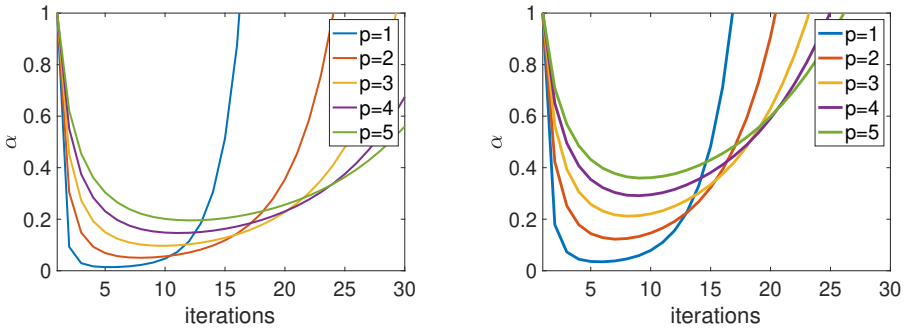

Fig. 12 Plots of α_k for F-GMRES New as a function of the number of iterations k for different values of p for Test 1 (on the left) and for Test 2 (on the right).

Figure 12 displays the parameters α_k for different values of p. Note that for all values of p, the sequence $\alpha_1, \alpha_2, \alpha_3, \ldots$ has the desired behavior: It decreases in the first few iterations, when little regularization is required, and increases in subsequent iterations when more regularization is needed. It can be seen that for larger values of p, the sequence $\{\alpha_k\}$ first decreases slower and then increases slower than for smaller values of p. Figure 13 displays how p affects the number of iterations required to satisfy the discrepancy principle and to determine the best restoration. We can see that more iterations are required for larger values of p. Moreover, Figure 13 shows that termination of the iterations with the discrepancy principle works well in the sense that the computed restorations are close to the best restorations.

The quality of the computed restorations is depicted in Figure 14. The blue curves show the RRE for the best restorations determined by F-GMRES for different values of p. These curves are quite insensitive to the choice of p. The red curves show the RRE when terminating the iterations with the discrepancy principle.

In conclusion, the numerical experiments of this section suggest that the value $p = 2$ is appropriate, because this value yields accurate restorations in a small number of iterations.

5 Conclusion

We have considered image deblurring when the point spread function is non-symmetric and anti-reflective boundary conditions are imposed. The use of standard Krylov subspace methods may require a substantial number of iterations. This can make the restoration of large images expensive. This paper describes a family of non-stationary structure-preserving preconditioners that are designed

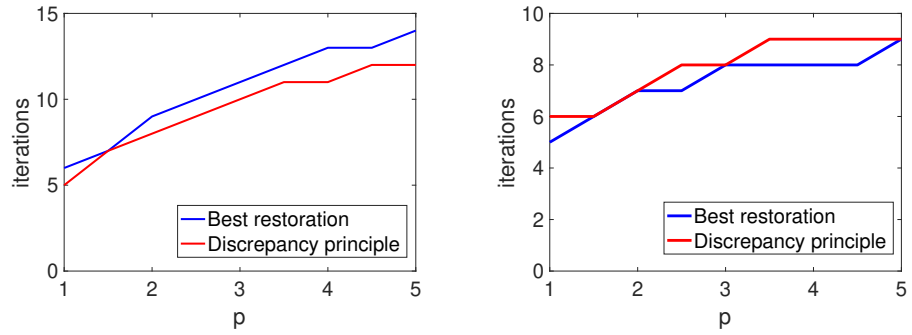

Fig. 13 Plot of the number of iterations required to compute the best restoration by F-GMRES New (blue curve) and plot of tthe numer of iterations required by F-GMRES New when using the discrepancy principle (red curve) as a function of p for Test 1 (on the left) and for Test 2 (on the right).

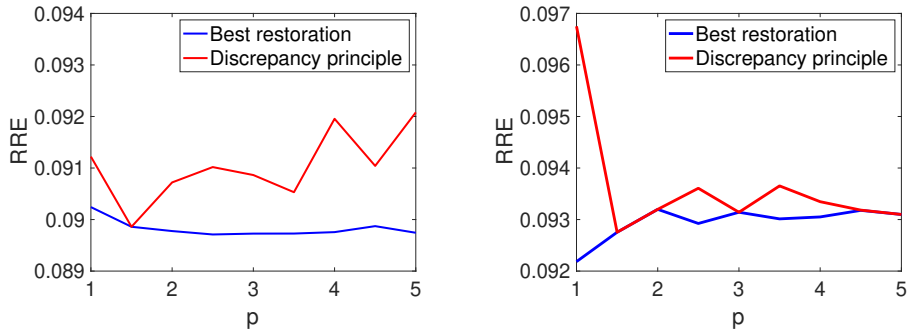

Fig. 14 Plot of the RRE for the best restoration determined by F-GMRES New (blue curve) and the restoration computed by F-GMRES New using the discrepancy principle (red curve) as a function of p for Test 1 (on the left) and for Test 2 (on the right).

to reduce the number of iterations. The parameters α_k that define the preconditioners are determined automatically during the iterations. We have focused on the application of these preconditioners in conjunction with the F-GMRES iterative method. Numerical results indicate that this solution approach is competitive with respect to the computational effort required and the quality of the computed restorations.

Acknowledgments

We would like to thank the referees and the editor for their valuable comments and suggestions, which helped us to improve the readability and the content of the paper. The first two authors are members of the INdAM Research group GNCS, which has partially supported this work. Research by the third author is supported by NSF grants DMS-1720259 and DMS-1729509. Part of the work of

the third author was carried out during a visit to Como. He would like to thank the second author for making this visit possible and enjoyable.

References

1. A. Aricò, M. Donatelli, J. Nagy, and S. Serra–Capizzano, *The anti-reflective transform and regularization by filtering*, in Numerical Linear Algebra in Signals, Systems, and Control, Lecture Notes in Electrical Engineering, vol. 80, Springer, 2011, pp. 1–21.
2. Å. Björck, *Numerical Methods for Least Squares Problems*, SIAM, Philadelphia, 1996.
3. A. Buccini, M. Donatelli, and L. Reichel, *Iterated Tikhonov regularization with a general penalty term*, Numer. Linear Algebra Appl., 24 (2017), e2089 (12 pages).
4. A. Buccini, Y. Park, and L. Reichel, *Deblurring methods using antireflective boundary conditions*, Appl. Math. Comput., 337 (2018), pp. 386–398.
5. M. Christiansen and M. Hanke, *Deblurring methods using antireflective boundary conditions*, SIAM J. Sci. Comput., 30 (2008), pp. 855–872.
6. P. Dell'Acqua, *A note on Taylor boundary conditions for accurate image restoration*, Adv. Comput. Math., 43 (2017), pp. 1283–1304.
7. P. Dell'Acqua, M. Donatelli, and C. Estatico, *Preconditioners for image restoration by reblurring techniques*, J. Comput. Appl. Math., 272 (2014), pp. 313–333.
8. P. Dell'Acqua, M. Donatelli, C. Estatico, and M. Mazza, *Structure preserving preconditioners for image deblurring*, J. Sci. Comput., 72 (2017), pp. 147–171.
9. P. Dell'Acqua, M. Donatelli, S. Serra Capizzano, D. Sesana, C. Tablino Possio, *Optimal preconditioning for image deblurring with anti-reflective boundary conditions*, Linear Algebra Appl., 502 (2016), pp. 159–185.
10. P. Dell'Acqua, F. Durastante, *New periodicontinuous boundary conditions for fast and accurate image restoration*, Adv. Comput. Math., 43 (2017), pp. 1283–1304.
11. M. Donatelli, C. Estatico, A. Martinelli, and S. Serra–Capizzano, *Improved image deblurring with anti-reflective boundary conditions and re-blurring*, Inverse Problems, 22 (2006), pp. 2035–2053.
12. M. Donatelli and M. Hanke, *Fast nonstationary preconditioned iterative methods for ill-posed problems with application to image deblurring*, Inverse Problems, 29 (2013), 095008 (16 pages).
13. M. Donatelli, C. Estatico, J. Nagy, L. Perrone, and S. Serra–Capizzano, *Anti-reflective boundary conditions and fast 2D deblurring models*, in Advanced Signal Processing Algorithms, Architectures, and Implementations XIII, ed. F. T. Luk, Proc. SPIE, vol. 5205, 2003, pp. 380–389.
14. M. Donatelli, D. Martin, and L. Reichel, *Arnoldi methods for image deblurring with anti-reflective boundary conditions*, Appl. Math. Comput., 253 (2015), pp. 135–150.
15. M. Donatelli and S. Serra–Capizzano, *Anti-reflective boundary conditions for deblurring problems*, J. Electr. Comput. Engng, 2010 (2010), Article ID 241467 (18 pages).
16. L. Dykes, F. Marcellán, and L. Reichel, *The structure of iterative methods for symmetric linear discrete ill-posed problems*, BIT, 54 (2014), pp. 129–145.
17. L. Dykes, S. Noschese, and L. Reichel, *Circulant preconditioners for discrete ill-posed Toeplitz systems*, Numer. Algorithms, 75 (2017), pp. 477–490.
18. Y. W. Fan and J. G. Nagy, *Synthetic boundary conditions for image deblurring*, Linear Algebra Appl., 434 (2011), pp. 2244–2268.
19. S. Gazzola and J. G. Nagy, *Generalized Arnoldi-Tikhonov method for sparse reconstruction*, SIAM J. Sci. Comput., 36 (2014), pp. B225–B247.
20. S. Gazzola, S. Noschese, P. Novati, and L. Reichel, *Arnoldi decomposition, GMRES, and preconditioning for linear discrete ill-posed problems*, Appl. Numer. Math., 142 (2019), pp. 102–121.
21. S. Gazzola, P. Novati, and M. R. Russo, *On Krylov projection methods and Tikhonov regularization*, Electron. Trans. Numer. Anal., 44 (2015), pp. 83–123.
22. M. Hanke and J. G. Nagy, *Restoration of atmospherically blurred images by symmetric indefinite conjugate gradient techniques*, Inverse Problems, 12 (1996), pp. 157–173.
23. M. Hanke, J. Nagy, and R. Plemmons, *Preconditioned iterative regularization for ill-posed problems*, in Numerical Linear Algebra, eds. L. Reichel, A. Ruttan, and R. S. Varga, de Gruyter, Berlin, 1993, pp. 141–163.

24. P. C. Hansen, J. Nagy, and D. P. O'Leary, *Deblurring Images Matrices, Spectra and Filtering*, SIAM Publications, Philadelphia, 2005.
25. T. A. Hearn and L. Reichel, *Extensions of the Justen–Ramlau blind deconvolution method*, Adv. Comput. Math., 39 (2013), pp. 465–491.
26. J. Huang, M. Donatelli, and R. H. Chan, *Nonstationary iterated thresholding algorithms for image deblurring*, Inverse Problems & Imaging, 7 (2013), pp. 717–736.
27. K. Morikuni, L. Reichel, and K. Hayami, *FGMRES for linear discrete ill-posed problems*, Appl. Numer. Math., 75 (2014), pp. 175–187.
28. M. Ng, R. H. Chan, and W. C. Tang, *A fast algorithm for deblurring models with Neumann boundary conditions*, SIAM J. Sci. Comput., 21 (1999) pp. 851–866.
29. S. J. Reeves, *Fast image restoration without boundary artifacts*, IEEE Trans. Image Process., 14 (2005), pp. 1448–1453.
30. Y. Saad, *A flexible inner-outer preconditioned GMRES algorithm*, SIAM J. Sci. Comput., 14 (1993), pp. 461–469.
31. Y. Saad, *Iterative Methods for Sparse Linear Systems*, 2nd ed., SIAM, Philadelphia, 2003.
32. Y. Saad and M. H. Schulz, *GMRES: A generalized minimal residual method for solving nonsymmetric linear systems*, SIAM J. Sci. Stat. Comput., 7 (1986), pp. 856–869.
33. S. Serra–Capizzano, *A note on anti-reflective boundary conditions and fast deblurring models*, SIAM J. Sci. Comput., 25 (2003), pp. 1307–1325.